Journal of Electronic Testing (2023) 39:597–609
https://doi.org/10.1007/s10836-023-06082-7

Identification of Unknown Electromagnetic Interference Sources Based on Siamese-CNN

Ying-Chun Xiao[1,2] · Feng Zhu[2] · Shengxian Zhuang[2] · Yang Yang[2]

Received: 28 November 2022 / Accepted: 30 August 2023 / Published online: 12 October 2023

Abstract
The prerequisite for promptly locating electromagnetic interference sources (EMIS) is the identification of EMIS. This research provides a new method for EMIS identification based on Siamese-CNN. A new convolutional neural network (CNN) structure is developed to extract the features of the EMIS. The symmetrical Siamese is adopted to enhance the number of training samples. The similarity metric of Siamese and the CNN-based subnetwork are merged in order to increase the similarity of samples from the same class and the differences between samples from different classes. A new loss function based on contrastive loss and cross-entropy loss is proposed to increase classification accuracy and discover unknown EMIS. The spectrums of EMIS are used as experimental datasets. The results show that the proposed method based on Siamese-CNN is resilient and has good generalization for training sets of various sizes. The identification accuracy for known EMIS can reach 100%, and the identification accuracy for unknown EMIS is more than 90%.

Keywords Electromagnetic interference sources (EMIS) · Convolutional neural network (CNN) · Siamese structure · Feature extraction · Extraction of deep features · Loss function

1 Introduction

With the widespread application of radio technology, the electromagnetic environment has become more and more complex. Various electromagnetic radiation sources (EMRS) have appeared. When the working frequency of the EMRS is equal to or very close to the working frequency of the electronic device or system, and the amplitude reaches a certain value, it will affect its normal operation. Previous studies have shown that electronic devices can be interfered with by electromagnetic emission signals, causing equipment or system failure [10, 15]. Many electronic devices and systems have weak anti-interference abilities against high-power electromagnetic (HPEM) sources [2, 11]. Current positioning technology can only determine the approximate range of the electromagnetic interference sources (EMIS), and it often takes a long time to find it. The EMIS identification can narrow the range and improve the positioning efficiency.

One kind of EMIS identification method is based on a theoretical model. Axell et al. proposed an online classification method for identifying noise signals by establishing models of emission source signals and noise signals [1]. Paoletti proposed an identification method based on modulation frequency analysis to identify broadband radiation sources by comparing the modulation frequency diagrams of the interfered device and the radiation source [22]. Aiming at the problem of different confidence levels of the radiation signals obtained by different sensors, the authors of [12] proposed an identification method based on the combination of Dempster-Shafer (DS) evidence theory and intuitionistic fuzzy sets. These identification methods are based on theoretical models in which the form of the radiation signal is either known or proposed under particular conditions, which have limits.

Another kind of EMIS identification method is based on feature extraction and classification methods. The authors of [36] use the Hilbert transform and empirical mode decomposition (EMD) to decompose the emission signal. They then use entropy, first-order moment, and second-order moment as feature vectors and support vector machine (SVM) to identify

Responsible Editor: S. Sindia

✉ Ying-Chun Xiao
1134748712@qq.com

[1] BaiLie School of Petroleum Engineering, Lanzhou City University, Lanzhou 730070, China

[2] School of Electrical Engineering, Southwest Jiaotong University, Chengdu 611756, China

the decomposed emission signal. The authors of [19] use time–frequency analysis to convert the radar radiation source signal into a two-dimensional grayscale image. The image's scale feature and location feature are then extracted, and the radar radiation source is identified using SVM. Satija et al. decomposed the emission signal using variational modal decomposition (VMD), calculated the entropy and moment as features, and used a K-NN classifier to identify the emitter [25]. A basic linear classifier and the VMD method are also used to identify the radar radiation sources in [6]. Many scholars have studied EMRS identification methods based on artificial neural networks (ANN), such as the back propagation (BP) neural network [27, 37]. Some scholars combine multiple types of signal characteristics and multiple classification methods to identify emitters [9, 28]. The accuracy of these methods is dependent on the feature or classification method. The feature extraction largely depends on people's experience and willingness, which is often time-consuming and results in some information loss.

With the development of machine learning in recent years, deep learning methods have promoted the research of EMIS identification methods. The authors of [16] proposed an end-to-end deep neural network, which uses convolutional neural networks (CNN) to extract spectrum features and identify complex radio signals. However, the end-to-end network directly learning high-dimensional data features requires more training time. The traditional CNN-based EMIS identification method extracts signal features using convolution and then classifies them using the Softmax classification layer [4, 30, 31]. To improve the classification ability of the Softmax classification layer, the loss function can be improved according to the characteristics of the interference source [23]. In addition, there have been radiation source identification methods based on AlexNet [18], generative adversarial network (GAN) [7], and long-short-term memory (LSTM) [20, 35]. The LSTM is used to process the time-domain signal of the radiation source. These identification methods based on deep learning require a large number of samples to get good identification accuracy. Although traditional CNN has good feature extraction capabilities, when the number of the training samples is small, a lot of network layers are needed and the convergence and timeliness are worse. The Siamese structure increases the number of training samples by constructing sample pairs. It can also be used to solve classification tasks where many classes or the number of classes is uncertain, but the number of training samples per class is small. The Siamese-CNN network is used for classification tasks and has shown promising results in other fields [5, 24, 29, 33, 34]. We have researched the CNN-based EMIS identification method [32]. However, it can only deal with all classes that are known ahead of time. When new classes are introduced, the network must be retrained.

In response to these problems, this paper proposes a new EMIS identification method based on Siamese structure and CNN, the main contributions are summarized as follows:

A new CNN-based subnetwork is proposed. A data processing layer is added to the subnetwork structure to extract more separable feature vectors.

A new loss function based on contrastive loss and cross-entropy loss is proposed to increase classification accuracy and detect unknown EMIS.

The remainder of the paper is organized as follows: Section 2 briefly reviewed the related work of CNN and Siamese. The proposed method is described in Section 3. Section 4 shows experiment results, and conclusions are drawn in Section 5.

2 Related Work

2.1 CNN

In 1990, Yann LeCun and others who worked in the AT & T laboratory proposed the structure of modern CNN [17]. A CNN mainly consists of several convolutional (Conv) layers, activation layers, pooling layers, and fully connected (FC) layers. CNN has the advantages of parameter sharing and sparsity of connections. It can reduce computational complexity, suppress over-fitting, and effectively extract signal features.

The convolutional layer is the core of the CNN. It can realize dimension reduction and feature extraction through "local connection" and "parameter sharing". The kernel size and stride of the convolution operation are fixed. Various features can be extracted by adjusting the parameters of the kernel. The combined use of multiple different kernels can improve the feature extraction ability of the network. Let $\boldsymbol{x}$ be the input vector of the convolutional layer, and its dimension is N_x. Let vector $\boldsymbol{k}$ be the convolution kernel, and its dimension is N_k. The result of the i-th one-dimensional convolution operation [38] is,

$$\boldsymbol{c}(i) = \sum_{n=1}^{N_k} \boldsymbol{x}(i+n) \times \boldsymbol{k}(n) \tag{1}$$

In some cases, the kernel dimension cannot be divided by the dimension of the input data, and some boundary data will not be able to participate in the convolution operation. Padding can make the dimension of the input data exactly match the dimension of the kernel, and the most widely used is zero-padding. Assuming that the number of padding is p and the stride is s, the vector dimension after convolution is

$$N_c = \left\lfloor \frac{N_x + 2p - N_k}{s} \right\rfloor + 1 \tag{2}$$

where ⌊⌋ means round down.

The activation layer performs nonlinear processing on the linear output of the previous layer. It enhances the characterization ability of the network through the activation function. The Rectified-Linear Unit (ReLU) activation function is used widely in CNN. It sets the neurons in the inhibited state to 0 to make the network becomes sparse, which can effectively alleviate the problems of gradient vanishing and over-fitting, and make the network converge fast.

Pooling integrates small-scale features to obtain new features, which is also called down-sampling. By reducing the vector dimension, the number of parameters is reduced, and the robustness of the neural network is greatly improved. Maximum pooling and average pooling are the most commonly used.

The FC layer is the final layer of CNN, which generally uses the Softmax activation function to achieve classification. Assuming that the FC layer is the l-th layer of the CNN, its input $\boldsymbol{A}^{[l-1]}$ is the output of the previous layer. Its output $\boldsymbol{A}^{[l]}$ is

$$\boldsymbol{A}^{[l]} = \mathrm{ReLU}\left(\boldsymbol{A}^{[l-1]} \cdot \boldsymbol{W}^{[l]} + \boldsymbol{B}^{[l]}\right) \tag{3}$$

where $\boldsymbol{W}^{[l]}$ is the weight matrix, $\boldsymbol{B}^{[l]}$ is the bias matrix, ReLU is nonlinear activation function.

The loss is the difference between the output value and the expected value of the network. The layer-to-layer connection is called "forward propagation." Then calculate the derivative of the loss function concerning each parameter and feedback the error layer by layer. The process of updating network parameters with optimization algorithms is called "back propagation." The network's training is finished after many forward and back propagation until the model's loss converges. In practical applications, CNNs with different structures are constructed according to different task requirements.

2.2 Siamese Network

The Siamese structure is a symmetrical structure composed of two identical neural networks in parallel, and all parameters in the two networks are shared. It uses a similarity metric to narrow the loss between samples of the same class and enlarge the loss between samples of different classes [3]. Figure 1 shows the Siamese structure, $(\boldsymbol{x}_1, \boldsymbol{x}_2)$ is the input sample pair, and y is the label. When $\boldsymbol{x}_1$ and $\boldsymbol{x}_2$ belong to the same class, it is called a positive sample pair, and the corresponding label y is 0. When $\boldsymbol{x}_1$ and $\boldsymbol{x}_2$ belong to different classes, it is called a negative sample pair, and the y is 1. N_1 and N_2 are two identical networks, and $\boldsymbol{w}$ is a shared parameter. $\boldsymbol{f}_1$ and $\boldsymbol{f}_2$ are the feature vectors obtained by the nonlinear mapping of the two samples through the network. $D()$ is the similarity function, which is used to measure the similarity between two feature vectors.

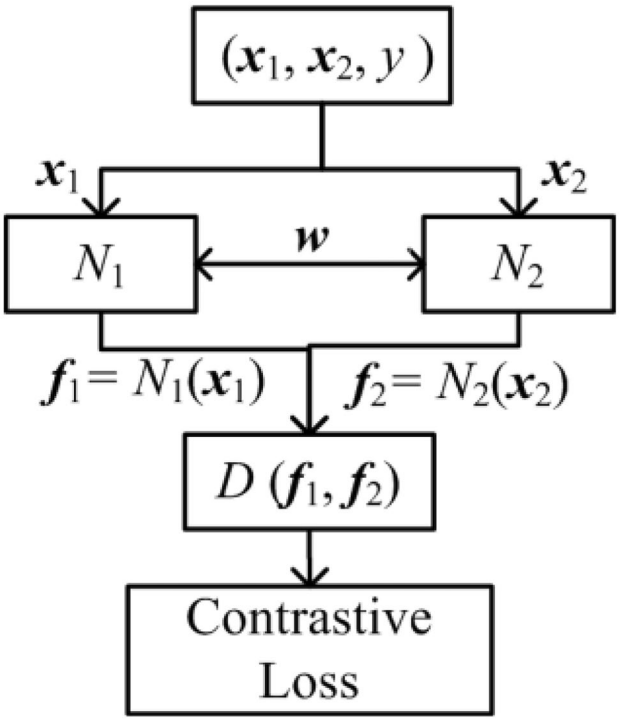

Fig. 1 Siamese architecture

The contrastive loss function was proposed by Chopra et al. [3], which is expressed as follows:

$$L(\boldsymbol{w}) = \sum_{i=1}^{P} L\left(\left(\boldsymbol{x}_1, \boldsymbol{x}_2, y\right)^i, \boldsymbol{w}\right) \tag{4}$$

$$\begin{aligned} L\left(\left(\boldsymbol{x}_1, \boldsymbol{x}_2, y\right)^i, \boldsymbol{w}\right) = (1-y) \cdot L_P\left(D\left(\boldsymbol{f}_1, \boldsymbol{f}_2\right)^i\right) \\ + y \cdot L_N\left(D\left(\boldsymbol{f}_1, \boldsymbol{f}_2\right)^i\right) \end{aligned} \tag{5}$$

It can be seen that when the contrastive loss function is minimized, the L_P is minimized, and the L_N is maximized. That is to say, when two input samples are similar, the feature vectors are also similar; when the two input samples are different, the feature vectors are also different.

3 The Proposed Work

3.1 The General Framework

The CNN and Siamese structures served as inspiration for this design. We constructed a new Siamese-CNN structure to extract the features of EMIS and identify them. The general framework of the new Siamese-CNN is shown in Fig. 2. It is composed of four parts, which are data preprocessing, feature extraction, similarity metric, and EMIS identification.

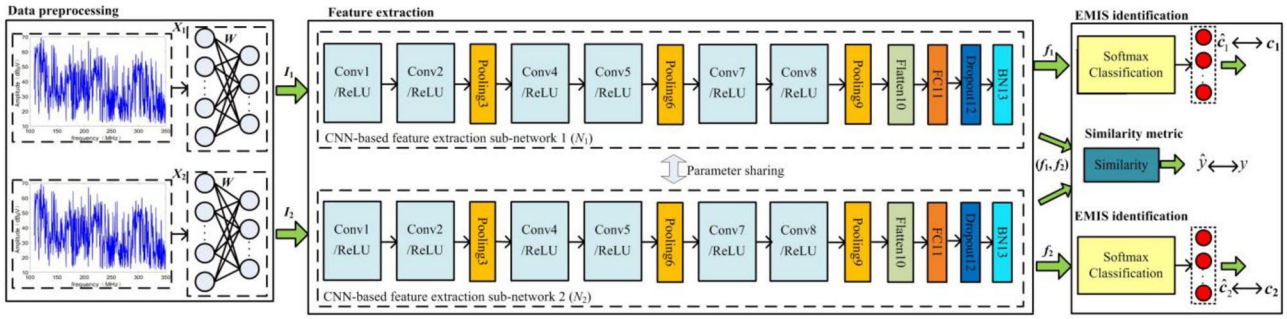

Fig. 2 The general framework of Siamese-CNN

$(\boldsymbol{x}_1, \boldsymbol{x}_2)$ is the input of network, and $(y, \boldsymbol{c}_1, \boldsymbol{c}_2)$ is the output label. $\boldsymbol{c}_1$ and $\boldsymbol{c}_2$ are one-hot vectors whose dimension is the number of classes. Suppose $\boldsymbol{x}_1$ is sample vector of a known class, and $\boldsymbol{x}_2$ is sample vector of an unknown class. If output y is 1, it means that $\boldsymbol{x}_2$ is different from $\boldsymbol{x}_1$ and is a new EMIS, that is, $\boldsymbol{c}_1 \neq \boldsymbol{c}_2$. If y is 0, then $\boldsymbol{x}_2$ and $\boldsymbol{x}_1$ are of the same class, that is, $\boldsymbol{c}_1 = \boldsymbol{c}_2$. The relationship between output labels is shown in Table 1. Therefore, it is necessary to propose a new loss function to train the new network and obtain the best parameters. The details will be introduced in 3.4 and 3.5.

3.2 Data Preprocessing

Take the spectrum of EMIS and background noise as samples, and input to the network. The data preprocessing denoises and normalizes the acquired spectral samples. To start, select any two samples from the same class as a positive sample pair and select any two samples from different classes as a negative sample pair. All the collected samples are generated into sample pairs. Divide them into training sets and test sets, where the training set accounts for 70% of the total and the test set accounts for 30%. The EMIS spectrum obtained by the actual test contains not only the components of the EMIS but also the components of other noises in the environment. A correlation operation can measure the similarity of two sequence signals. The correlation calculation results of different EMIS spectrums and the same background noise can highlight the difference between EMIS signals. An FC layer is used to achieve noise reduction and normalization of the test data. Let the background noise vector be the weight, then the output of the i-th sample pair after data preprocessing is

$$\begin{cases} \boldsymbol{h}_1^i(j) = Sigmoid\left(\boldsymbol{x}_1^i(j) \cdot \boldsymbol{b}(j)\right) \\ \boldsymbol{h}_2^i(j) = Sigmoid\left(\boldsymbol{x}_2^i(j) \cdot \boldsymbol{b}(j)\right) \end{cases} \tag{6}$$

where, $1 \leq j \leq m$, m is the length of each sample. The sample data is converted to a value between 0 and 1 through the Sigmoid activation function to complete the normalization process. The weight vector $\boldsymbol{b}$ is composed of background noise, which is not needed to be trained. The preprocessed samples take into account the background noise, which reduces the dependence of the EMIS sample data on the background noise.

Table 1 The relationship between output labels

$(\boldsymbol{x}_1, \boldsymbol{x}_2)$	y	$(\boldsymbol{c}_1, \boldsymbol{c}_2)$
$\boldsymbol{x}1$ and $\boldsymbol{x}2$ are of different classes	1	$\boldsymbol{c}_1 \neq \boldsymbol{c}_2$
$\boldsymbol{x}1$ and $\boldsymbol{x}2$ are of the same class	0	$\boldsymbol{c}_1 = \boldsymbol{c}_2$

3.3 Feature Extraction

The feature extraction part is composed of two CNN-based subnetworks. The structure of the two sub-networks is the same, and their parameters are shared. Each sub-network consists of six convolutional layers with ReLU, three maximum pooling layers, one flattening layer, one FC layer, one dropout layer, and one batch normalization (BN) layer. The convolutional layer includes a convolution operation and a nonlinear activation operation with an activation function of ReLU. The maximum value of the EMIS spectrum can better reflect the interference characteristics, so we adopt the maximum pooling. The maximum pooling can enhance the generalization processing ability of the network. The higher the dimension of the feature vector after the convolution operation, the more it will affect the classification effect. It makes the network easy to fall into over-fitting and reduces the generalization ability. Therefore, dropout [14] is used in the FC layer to let neurons work randomly according to a certain probability (keep_prob). The non-working neuron will not calculate its parameters during the training, nor will it be too sensitive to the neuron's information when the model is learning. The model learns and extracts relevant features based on the information of other working neurons to prevent over-fitting. Because only some neurons work, the complexity of network calculation is reduced and the training speed of the model is improved.

As the network layers increase, the input distribution of the hidden layer gradually deviates. Standardizing the features can avoid the problem of the neuron node gradient vanishing during back propagation. BN [8] can speed up the training process, avoid excessive reliance on initial values, and suppress over-fitting, especially for small datasets. The output of the FC layer is the feature vector. The t-distribution stochastic neighbor embedding (t-SNE) algorithm [21] can visualize features.

3.4 Similarity Metric

The network training is to continuously update the network parameters so that the loss reaches the expected minimum value more smoothly and quickly and obtains the distinguishable feature vector. Therefore, it requires reducing the loss between samples of the same class and enlarging the loss between samples of different classes. The similarity metric of two feature vectors can be expressed by the contrastive loss function, which can be defined as

$$L\left(\left(\boldsymbol{x}_1,\boldsymbol{x}_2,y\right),\boldsymbol{w}\right)=\frac{1}{2N}\sum_{n=1}^{N}(1-y)\cdot L_P+y\cdot L_N \tag{7}$$

where N is the number of sample pairs. L_P is the loss between the feature vectors $\boldsymbol{f}_1$ and $\boldsymbol{f}_2$ from the same class. L_N is the loss between feature vectors $\boldsymbol{f}_1$ and $\boldsymbol{f}_2$ from two different classes. L_P and L_N are defined as

$$L_P=D\left(\boldsymbol{f}_1,\boldsymbol{f}_2\right)^2=\left(\left\|\boldsymbol{f}_1-\boldsymbol{f}_2\right\|_2\right)^2=\sum_{i=1}^{P}\left(\boldsymbol{f}_1^i-\boldsymbol{f}_2^i\right)^2 \tag{8}$$

$$L_N=\max\left[\left(\eta-D\left(\boldsymbol{f}_1,\boldsymbol{f}_2\right)\right),0\right]^2 \tag{9}$$

where P is the dimension of the feature vector. The network is trained to make the L_P and L_N as small as possible. The L_P is trained to be close to 0, that is, two feature vectors are very similar. η is a threshold. If $D\left(\boldsymbol{f}_1,\boldsymbol{f}_2\right)$ is less than η, the network is trained to make the value of $D\left(\boldsymbol{f}_1,\boldsymbol{f}_2\right)$ increase to η, thus increasing the difference between the two feature vectors. If η is set too small, the difference between negative samples is not obvious, and if η is too large, the minimization process of L_N takes more time. We proposed a method to determine the η. The η defined as the maximum distance between all class centers, i.e.

$$\eta=\max_{1\le i,j\le K,i\ne j}\left\|\boldsymbol{\mu}_i-\boldsymbol{\mu}_j\right\|_2 \tag{10}$$

where $\boldsymbol{\mu}_i$ and $\boldsymbol{\mu}_j$ are the class centers of the two feature vector.

When the two input samples are of the same class, the derivative of the contrastive loss function concerning the weight $\boldsymbol{w}$ is

$$\frac{\partial L}{\partial \boldsymbol{w}}=\frac{1}{\mathrm{N}}\sum_{n=1}^{\mathrm{N}}D\left(\boldsymbol{f}_1,\boldsymbol{f}_2\right)\cdot\frac{\partial D\left(\boldsymbol{f}_1,\boldsymbol{f}_2\right)}{\partial \boldsymbol{w}} \tag{11}$$

When the two input samples belong to different classes, the derivative of the contrastive loss function concerning the weight $\boldsymbol{w}$ is

$$\frac{\partial L}{\partial \boldsymbol{w}}=-2\left[\eta-D\left(\boldsymbol{f}_1,\boldsymbol{f}_2\right)\right]\cdot\frac{\partial D\left(\boldsymbol{f}_1,\boldsymbol{f}_2\right)}{\partial \boldsymbol{w}} \tag{12}$$

where $\frac{\partial D\left(\boldsymbol{f}_1,\boldsymbol{f}_2\right)}{\partial \boldsymbol{w}}$ is

$$\frac{\partial D\left(\boldsymbol{f}_1,\boldsymbol{f}_2\right)}{\partial \boldsymbol{w}}=\frac{\left(\sum_{i=1}^{P}\left(\boldsymbol{f}_1^i-\boldsymbol{f}_2^i\right)\cdot\left(\frac{\partial \boldsymbol{f}_1^i}{\partial \boldsymbol{w}}-\frac{\partial \boldsymbol{f}_2^i}{\partial \boldsymbol{w}}\right)\right)}{\sqrt{\sum_{i=1}^{P}\left(\boldsymbol{f}_1^i-\boldsymbol{f}_2^i\right)^2}} \tag{13}$$

After the derivative of the contrastive loss function with respect to each parameter is calculated, the optimization algorithm can be used to update the parameters until the comparison loss function converges. It can be seen that when the contrastive loss function converges to 0, the features of the same class are more compact, and the features between different classes are more dispersed, so that the feature distribution is optimal.

3.5 EMIS Identification

As shown in Fig. 2, the input of the EMIS identification part is the feature vector, and the output is the vector composed of the probability distribution of the feature vector on each class and the similarity between $\boldsymbol{f}_1$ and $\boldsymbol{f}_2$, which can be expressed as

$$\hat{\boldsymbol{c}}=\left[\hat{c}_{11},\hat{c}_{12}\cdot\cdot,\hat{c}_{1i}\cdot\cdot,\hat{c}_{1C},\hat{y},\cdot\cdot,\hat{c}_{21},\hat{c}_{22}\cdot\cdot,\hat{c}_{2i}\cdot\cdot,\hat{c}_{2C}\right] \tag{14}$$

where C is the number of classes. The output label of the network is

$$\boldsymbol{c}=\left[c_{11},c_{12}\cdot\cdot,c_{1i}\cdot\cdot,c_{1C},y,\cdot\cdot,c_{21},c_{22}\cdot\cdot,c_{2i}\cdot\cdot,c_{2C}\right] \tag{15}$$

$\boldsymbol{c}$ is the vector after one-hot transformation, belonging to $\{0,1\}$. Take the N_1 network in Fig. 2 as an example to illustrate the process of softmax classification. Assuming that the weight and bias vector of this layer are $\boldsymbol{w}_1$ and $\boldsymbol{b}_1$, respectively, the result after linear calculation is

$$z_1=\boldsymbol{w}_1\cdot\boldsymbol{f}_1+\boldsymbol{b}_1 \tag{16}$$

Let $\hat{\boldsymbol{c}}_1$ represent the output of the softmax classification layer of N_1, then the i-th data in vector $\hat{\boldsymbol{c}}_1$ is

$$\hat{c}_{1i} = \frac{e^{z_{1i}}}{\sum_{i=1}^{C} e^{z_{1i}}} \tag{17}$$

where z_{1i} represents the i-th data in vector z_1.Through the activation function of (17), the maximum value in $\hat{\boldsymbol{c}}_1$ is highlighted, and the other values are significantly suppressed. The same method can be used to compute the output vector $\hat{\boldsymbol{c}}_1$ of N_2. $\hat{y}$ is the similarity of two feature vectors, expressed by Euclidean distance, i.e.

$$\hat{y} = D(\boldsymbol{f}_1, \boldsymbol{f}_2) \tag{18}$$

In order to identify the classes of EMIS represented by $\boldsymbol{f}_1$ and $\boldsymbol{f}_2$, the loss functions of N_1 and N_2 are obtained according to the cross entropy loss function, which can be expressed as

$$L_{CE-N_1} = -\sum_{i=1}^{C} c_{1i} \log \hat{c}_{1i} \tag{19}$$

$$L_{CE-N_2} = -\sum_{i=1}^{C} c_{2i} \log \hat{c}_{2i} \tag{20}$$

In order to determine whether $\boldsymbol{f}_1$ and $\boldsymbol{f}_2$ belong to the same class, the contrast loss function for unknown EMIS can be expressed as

$$L_{SM} = \frac{1}{2N} \sum_{n=1}^{N} \left((1-y) \cdot \hat{y}^2 + y \cdot \max^2 \left[(\eta - \hat{y}), 0 \right] \right) \tag{21}$$

For the sample pair $(\boldsymbol{x}_1, \boldsymbol{x}_2)$ of the test set, if $\boldsymbol{x}_1$ is the sample vector of the known EMIS, $\boldsymbol{x}_2$ is the sample vector of the EMIS to be identified. $\boldsymbol{x}_2$ can also be the sample vector of the unknown EMIS. The network is trained to make $\hat{y} = \eta$, which means that the EMIS to be identified is not the class of $\boldsymbol{x}_1$. Otherwise, the network is trained to make $\hat{y} = 0$, which means that the EMIS to be identified is the class of $\boldsymbol{x}_1$.

Therefore, the total loss function of the new Siamese-CNN network is defined as

$$Loss = \lambda_1 \cdot L_{SM} + \lambda_2 \left\{ \begin{array}{l} (1-y)\left(L_{CE-N_1} - L_{CE-N_2}\right) \\ +y \cdot \max\left[\left(\eta - \left(L_{CE-N_1} - L_{CE-N_2}\right)\right), 0\right]^2 \end{array} \right\} \tag{22}$$

where $\left(L_{CE-N_1} - L_{CE-N_2}\right)$ is the loss difference between the N_1 and the N_2. When y is 0, the smaller the difference, the better. When y is 1, the greater the difference, the better, and make the difference close to the threshold η. λ_1 and λ_2 are scalars that measure the contrastive loss and the difference between the two cross-entropy losses. The gradients of the new loss function concerning each parameter are calculated. The Adam optimization algorithm [13] is used to update the network parameters so that the total loss converged to a minimum value close to 0. The trained network can classify the trained EMIS and identify unknown EMIS.

4 Experiments

Figure 3 depicts the overall process of the new EMIS identification method suggested in this work. Network training and testing are included in the method. The simulation experiments are based on the actual spectrum of five EMIS and background noise.

We verify the comprehensive performance of the new method on various datasets and compare it with some existing methods. All experiments were carried out on a laptop equipped with an 11th Generation Intel (R) Core (TM) i5-1135G7 @ 2.40 GHz processor and an NVIDIA GeForce MX450 graphics card. The laptop has 16 GB of memory. The training and testing work was implemented using the open-source software framework TensorFlow.

4.1 Description of Datasets

We collected three classes of aging power supplies (aging power supply for civil lighting, aging power supply for airport lighting, and aging power supply for airport runway lighting) and two classes of signal jammers (PBQ2X and PBQ6X) as EMIS. Taking the electromagnetic environment of one airport in China as an example, the working frequency of the airport's communication and navigation equipment is mainly concentrated in the 108–2000 MHz range. We have conducted multiple tests on the emission signal of each EMIS in six frequency bands (108-148 MHz, 108-350 MHz,

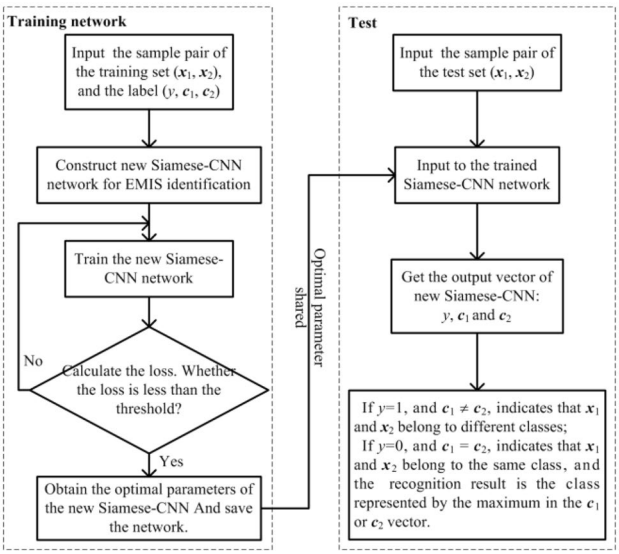

Fig. 3 The process of the new EMIS identification method

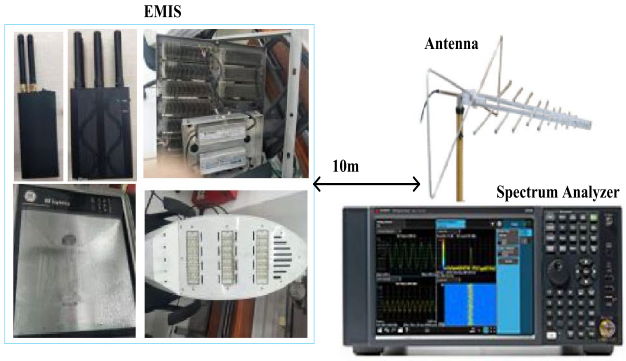

Fig. 4 Schematic diagram of test

310-350 MHz, 962-2000 MHz, 1010-1050 MHz, and 1070-1110 MHz). The test methods and experimental equipment are strictly implemented following the requirements of the standard CISPR 16–1 [26], and the test distance is 10 m. Test equipment includes a spectrum analyzer (N9010B EXA), a cable, and a corresponding receiving antenna, etc. Figure 4 is the schematic diagram of the test.

Through the test, it is found that the emission signal of the EMIS in the high frequency range is very weak, and its magnitude is almost the same as the background noise. The emission signals of EMIS are mainly concentrated at 108–350 MHz. Therefore, we repeated the test 20 times for the background noise and the emission signal of EMIS in this frequency band. That is, 20 samples were obtained for each class of signal, and the sample length of each sample was 1001. We label background noise, signal jammer-PBQ2X, signal jammer-PBQ6X, the aging power supply for civil lighting, the aging power supply for airport lighting, and the aging power supply for airport runway lighting as Class 0, Class 1, Class 2, Class 3, Class 4, and Class 5, respectively. One sample of background noise and each of the five classes of EMIS are shown in Fig. 5. It can be seen that the signal amplitudes of various EMIS are larger than the background noise, and the spectrum of some EMIS is relatively similar, so the characteristics are not obvious.

Take out 14 samples of Class 0, Class 1, Class 2, Class 3, Class 4 as the training set, and 6 samples as the test set. Class 5 is regarded as an unknown EMIS, and all of its 20 samples are used as the test set. Therefore, $5 \times C_{14}^2 = 455$ positive sample pairs and $C_5^2 \times 14 \times 14 = 1960$ negative sample pairs can be generated in training set, $5 \times C_6^2 + C_{20}^2 = 265$ positive sample pairs and $C_5^2 \times 6 \times 6 + C_5^1 \times C_6^1 \times C_{20}^1 = 960$ negative sample pairs can be generated in test set. To test the performance of the proposed method on various sized datasets as well as the identification performance of the unknown EMIS, we generated three datasets, as shown in Table 2. The number of negative sample pair is three times that of positive sample pair. Both dataset 1 and dataset 2 contain the unknown EMIS Class 5, but the number of their sample pairs is different. Dataset 3 is composed of the five classes of samples and does not contain the unknown EMIS Class 5.

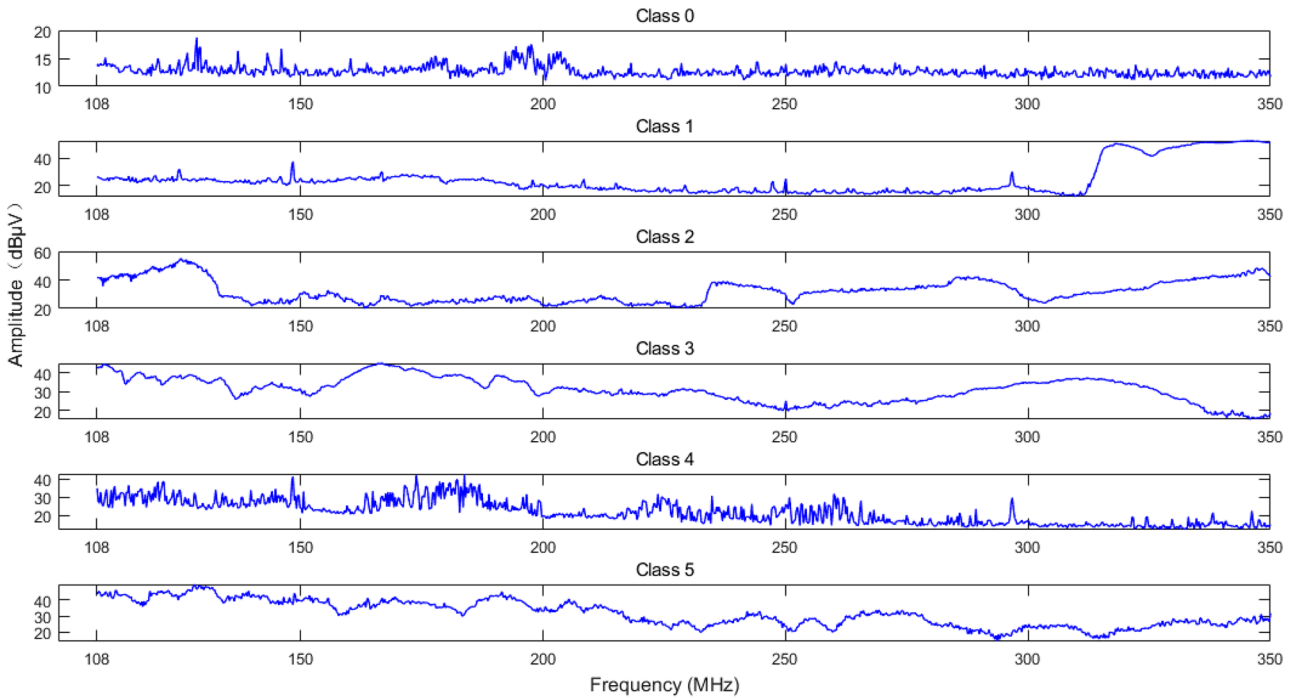

Fig. 5 One sample of background noise and five classes of EMIS

Table 2 Details of datasets

Dataset		The Number of positive sample pairs	The Number of negative sample pairs	Total
Dataset 1	Training set 1	120	360	480
	Test set 1	30	90	120
Dataset 2	Training set 2	455	1365	1820
	Test set 2	265	797	1062
Dataset 3	Training set 3	175	525	700
	Test set 3	75	225	300

4.2 Network Parameters

The new network is trained based on the training set and the parameters are updated so that the network achieves the best performance and finally obtains all the parameters. The parameters of the CNN-based sub-network are showed in Table 3.

The initialization method of all parameters is Xavier method, and the learning rate is set to 0.001. The batch size of the BN layer is set to 64, momentum is 0.99, and epsilon is 0.001. The number of neurons in the FC layer is set to 200, and the number of neurons in the Softmax classification layer is 5. The keep-prob of the Dropout layer is set to 0.5 during training and 1 during testing. The Adam optimization method is used, and β_1=0.9, β_2=0.999. The η and μ in the loss function are set to 2.5, and both λ_1 and λ_2 are set to 1. The sub-network has a total of 491,045 parameters, including 490,645 trainable parameters and 400 non-trainable parameters. When epochs are set to 200, the loss reaches a stable minimum value and we obtain the optimal parameters of the network.

4.3 Experimental Results

We use dataset 1 with the smallest number of samples to train and test the proposed EMIS identification method to verify its performance. In addition, the new Siamese-CNN in this paper is compared with some recent EMIS identification methods, and the evaluation indicators of various methods are obtained on three datasets.

4.3.1 Verification Experiment Results

Dataset 1 is used to train and test the new Siamese-CNN. Figure 6 shows the curve of training and test loss with epochs. At the end of training and testing, the stability of the loss curve is good, and there is no over-fitting or under-fitting.

The training and test accuracy of Siamese-CNN are shown in Fig. 7. It can be seen that as the number of training steps increases, the network is gradually optimized, and the training accuracy and test accuracy can reach 100% in the later stages.

To observe the feature vector more intuitively, we take out the output of the FC layer of the two sub-networks and use the t-SNE algorithm for visualization. Figure 8 shows the two-dimensional (2D) feature distribution of the sample pair formed by Siamese-CNN. It can be seen that the intra-class distance is much smaller than the inter-class distance, and the various classes are very different. This shows that the similarity metric of the new Siamese-CNN reduces the difference between similar samples, increases the difference between different classes of samples, and provides a basis for good classification.

Table 3 Feature extraction sub-network parameters

Layer	Related parameters	Output Shape	Parameters#
Conv1	filters = 16;size = 3;strides = 1	(996, 16)	64
Conv2	filters = 16;size = 3;strides = 1	(997, 16)	784
Max_Pooling3	filters = 16;size = 3;strides = 3	(332, 16)	0
Conv4	filters = 64;size = 3;strides = 1	(330, 64)	3136
Conv5	filters = 64;size = 3;strides = 1	(328, 64)	12352
Max_Pooling6	filters = 64;size = 3;strides = 3	(109, 64)	0
Conv7	filters = 64;size = 3;strides = 1	(107, 64)	12352
Conv8	filters = 64;size = 3;strides = 1	(105, 64)	12352
Max_Pooling9	filters = 64;size = 3;strides = 3	(35, 64)	0
Flatten10	None	2240	0
FC11	200	200	460900
Dropout12	keep-prob = 0.5	200	0
Batch Normalization13	batch size = 64	200	800
Softmax14	5	5	1005

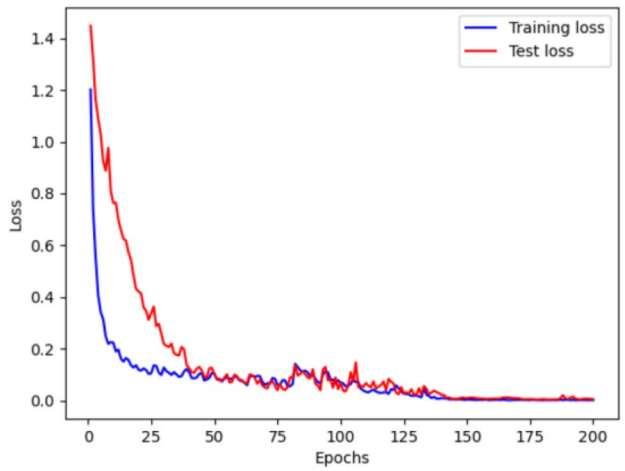

Fig. 6 The training and test loss of Siamese-CNN on the dataset 1

The test set 1 is used to test the trained Siamese-CNN. For the test sample pair (X_1, X_2), the possible class of X_1 is Class 0, Class 1, Class 2, Class 3, or Class 4, and X_1 has been trained. X_2 could, however, be a sample vector from an untrained unknown Class 5. The confusion matrix shown in Fig. 9 visually shows the identification result of the new Siamese-CNN on the test set 1. It can be seen that the classification accuracy of the new Siamese-CNN for known EMIS can reach 100%, the identification accuracy for unknown EMIS Class 5 is 90%, and the average identification accuracy is about 98.33%.

4.3.2 Comparative Experimental Results

First of all, the fully connected neural network (FC-NN), AlexNet, CNN, and unimproved Siamese-CNN are

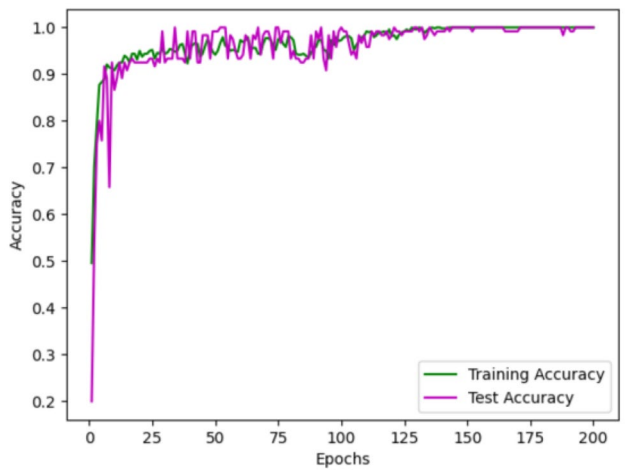

Fig. 7 The training and test accuracy of Siamese-CNN on the dataset 1

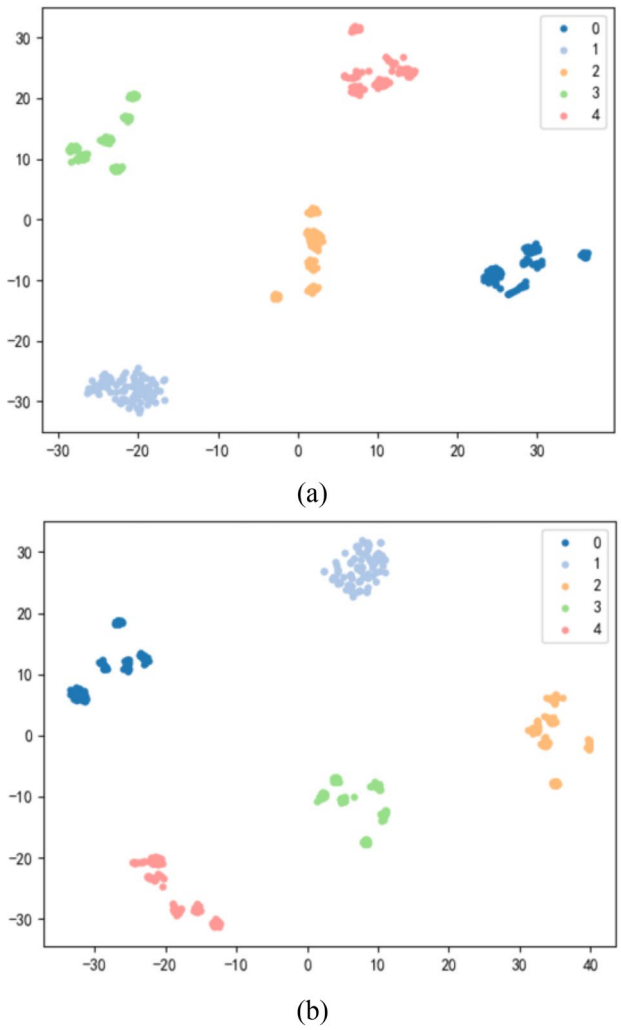

Fig. 8 2D feature distribution of the new Siamese-CNN on training set 1: **a** 2D features obtained by N_1 network, **b** 2D features obtained by N_2 network

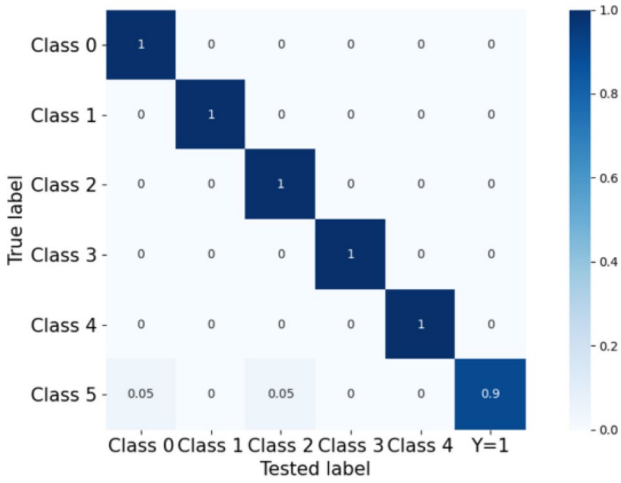

Fig. 9 The confusion matrix of the new Siamese-CNN on the test set 1

Table 4 Identification results of the four methods on the test set 1

Class	0	1	2	3	4	5
FC-NN	(80 ± 10)%	(85 ± 10)%	(90 ± 5)%	(90 ± 5)%	(90 ± 5)%	(0 ± 0)%
AlexNet	(90 ± 5)%	(100 ± 0)%	(100 ± 0)%	(100 ± 0)%	(95 ± 5)%	(0 ± 0)%
CNN	(95 ± 5)%	(100 ± 0)%	(100 ± 0)%	(100 ± 0)%	(100 ± 0)%	(0 ± 0)%
Unimproved Siamese-CNN	(95 ± 5)%	(100 ± 0)%	(100 ± 0)%	(100 ± 0)%	(100 ± 0)%	(85 ± 5)%
New Siamese-CNN	(100 ± 0)%	(100 ± 0)%	(100 ± 0)%	(100 ± 0)%	(100 ± 0)%	(95 ± 5)%

constructed. These methods do not require manual feature extraction and are currently popular identification methods.

FC-NN is a 5-layer network including three hidden layers. The number of neurons in each hidden layer is 25, 12, and 5, respectively. The activation function of the hidden layer is ReLU, and the activation function of the output layer is Sigmod. The cross-entropy loss function and the Adam optimization algorithm are used to update the parameters.

The AlexNet network includes five convolutional layers, five maximum pooling layers, five normalization layers, two FC layers, and one dropout layer. Each convolutional layer is followed by a maximum pooling layer and a normalization layer. Xavier is used as the initialization method, and Adam is used as the optimization method. This method replicates the classic AlexNet as much as possible.

CNN is the feature extraction sub-network based on CNN constructed in this paper. Unimproved Siamese-CNN consists of two CNNs and unimproved contrastive loss function.

Five networks are trained and tested on three datasets. The identification results (value ± deviation) of the four methods on the three test sets are shown in Tables 4, 5 and 6, respectively. In Tables 4 and 5, Class5 is unknown EMIS. As can be observed, FC-NN, AlexNet, and CNN cannot identify the class5 that has not been trained. The class5 is mistakenly identified as one of Class 0 ~ Class 4, resulting in poor average accuracy for these networks. New and unimproved Siamese -CNN are able to identify unknown EMIS. Because of the improved loss function, the new Siamese-CNN has improved the accuracy of unimproved Siamese-CNN for unknown EMIS in two data sets by 17.65% and 13.63%.

Table 6 shows that AlexNet, CNN, unimproved Siamese-CNN, and new Siamese-CNN have pretty high identification accuracy for known EMIS. The FC-NN is unable to extract the features of the original data effectively. Its identification accuracy is low. To improve its identification accuracy, its network depth and training set must be expanded, but there will be a large number of parameters to be trained. Although the classic AlexNet has good classification capabilities, the new CNN subnetwork is more suitable for the identification task of this article. From the identification results of the five methods on the three datasets, it can be seen that the more training samples, the higher the identification accuracy of each network. The identification accuracy of the new Siamese-CNN is higher than that of other methods, especially on the small dataset. The new Siamese-CNN has an identification accuracy of 100% for known EMIS, which increases the average identification accuracy of FC-NN, AlexNet, and CNN by 9.09%, 2.04%, and 1.52%, respectively. The new Siamese-CNN also has an identification accuracy of over 90% for unknown EMIS.

Ten experiments were performed on the test set and the average identification accuracy was calculated. The ROC curves for each method on dataset 1 are reported in Fig. 10. The AUC of our new Siamese-CNN is 1 on the smaller test set 1, which is 0.08, 0.02, 0.02, and 0.02 larger than that of FC-CNN, AlexNet, CNN, unimproved Siamese-CNN, respectively. The larger AUC of the new Siamese-CNN represents the better network performance.

Figure 11 shows the F1 scores of different methods on different sized data sets. From Fig. 11, the F1 scores increase with the increase of training samples for each class. The proposed new Siamese-CNN has larger F1 scores on data sets of different sizes. This shows that in the case of a limited number of training samples, the new Siamese-CNN can better identify the EMIS.

In addition, the number of parameters that the new Siamese-CNN needs to train is similar to that of CNN, about 490,645. To show the efficiency of the new Siamese-CNN, the

Table 5 Identification results of the four methods on the test set 2

Class	0	1	2	3	4	5
FC-NN	(91.53 ± 0.56)%	(96.04 ± 1.13)%	(96.61 ± 1.69)%	(95.48 ± 2.26)%	(92.66 ± 0.56)%	(0 ± 0)%
AlexNet	(97.74 ± 0.56)%	(100 ± 0)%	(100 ± 0)%	(100 ± 0)%	(98.31 ± 0.56)%	(0 ± 0)%
CNN	(98.87 ± 1.13)%	(100 ± 0)%	(100 ± 0)%	(100 ± 0)%	(100 ± 0)%	(0 ± 0)%
Unimproved Siamese-CNN	(98.93 ± 0.3)%	(100 ± 0)%	(100 ± 0)%	(100 ± 0)%	(100 ± 0)%	(87.01 ± 0.66)%
New Siamese-CNN	(100 ± 0)%	(100 ± 0)%	(100 ± 0)%	(100 ± 0)%	(100 ± 0)%	(98.87 ± 1.13)%

Table 6 Identification results of the four methods on the test set 3

Class	0	1	2	3	4
FC-NN	(90 ± 1.67)%	(95 ± 3.33)%	(95 ± 1.67)%	(95 ± 3.33)%	(91.67 ± 3.33)%
AlexNet	(96.67 ± 1.67)%	(100 ± 0)%	(100 ± 0)%	(100 ± 0)%	(98.33 ± 1.67)%
CNN	(98.33 ± 1.67)%	(100 ± 0)%	(100 ± 0)%	(100 ± 0)%	(100 ± 0)%
Unimproved Siamese-CNN	(98.51 ± 1.05)%	(100 ± 0)%	(100 ± 0)%	(100 ± 0)%	(100 ± 0)%
New Siamese-CNN	(100 ± 0)%	(100 ± 0)%	(100 ± 0)%	(100 ± 0)%	(100 ± 0)%

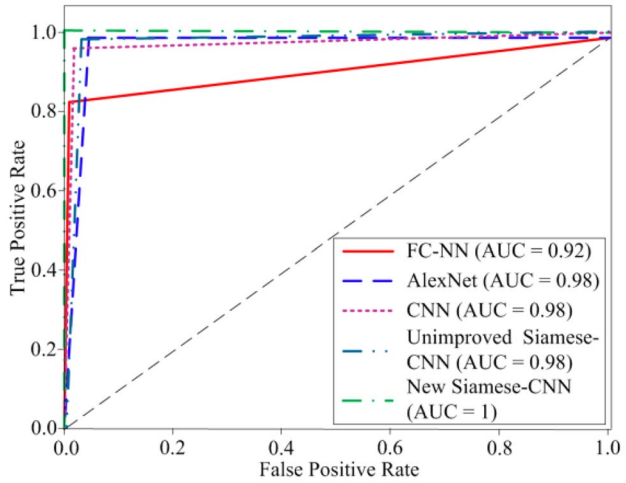

Fig. 10 The ROC curves for each method on dataset 1

training time of different methods for each sample are show in Table 7. The average running time of the new Siamese-CNN for each sample is about 0.01 s, including the time for data preprocessing, feature extraction, backward propagation, and final classification. It can be seen that the training time of CNN, unimproved Siamese-CNN, and new Siamese-CNN is similar and the shortest. However, the identification accuracy of new Siamese-CNN is the highest. Therefore, the performance of the new Siamese-CNN is the best.

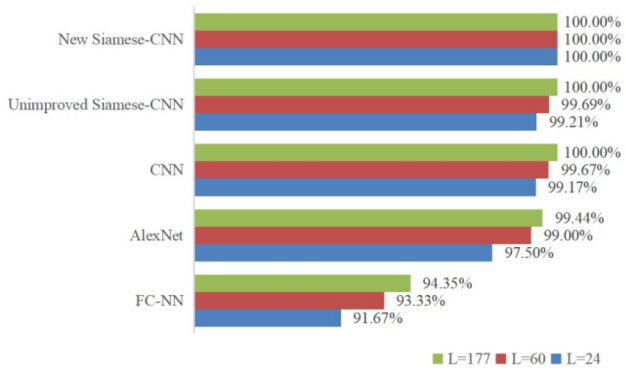

Fig. 11 F1 scores of different methods (L is the number of test samples for each class)

Table 7 The training time of different methods for each sample

Networks	Training time for each sample (s)
FC-NN	0.041
AlexNet	0.015
CNN	0.009
Unimproved Siamese-CNN	0.011
New Siamese-CNN	0.010

5 Conclusion and Outlook

In this paper, we proposed a new Siamese-CNN for EMIS identification. The Siamese structure augments the training set samples with asymmetric network structure. The similarity metric and the CNN-based subnetwork make the sample features of the same class more similar, and the sample features of different classes more discrete. Their combination makes the feature distribution better and provides a basis for accurate identification. The new Siamese-CNN combines the contrastive loss function and the cross-entropy loss function to improve the classification ability and detect the unknown EMIS. The comprehensive performance of the new Siamese-CNN is verified through verification experiments and comparative experiments on three datasets. It is also possible to train a well-performing Siamese-CNN with small datasets. The classification accuracy of the new Siamese-CNN for known EMIS can reach 100%, and the identification accuracy for unknown EMIS can reach more than 90%.

The proposed new Siamese-CNN performs well in identifying single EMIS, but is unable to identify multiple EMIS simultaneously. Although it needs to be further developed, we hope that our method can provide some inspiration for research in other classification and recognition fields. The dataset in this paper is a single type of EMIS spectrum. In future work, we will collect more types of information about the EMIS, further improve and verify our algorithm, and investigate methods to identify multiple EMIS.

Funding This work is supported by National Key R&D Program of China (No. 2018YFC0809500).

Data Availability The datasets generated during and/or analysed during the current study are available from the corresponding author on reasonable request.

Declarations

Conflict of Interest I certify that there is no actual or potential conflict of interest in relation to this article.

References

1. Axell E, Tengstrand SÖ, Wiklundh K (2017) Online classification of class a impulse interference. Proc IEEE Military Commun Conf 180–184
2. Brauer F, Sabath F, Haseborg JL (2009) Susceptibility of IT network systems to interference by HPEM. Proc IEEE Int Symp Electromagn Compat 237–242
3. Chopra S, Hadsell R, LeCun Y (2005) Learning a similarity metric discriminatively, with application to face verification. Proc IEEE Comput Soc Conf Comput Vis Pattern Recognit 539–546
4. Ding L, Wang S, Wang F, Zhang W (2018) Specific emitter identification via convolutional neural networks. IEEE Commun Lett 22(12):2591–2594
5. Gao J, Xu L, Bouakaz A, Wan M (2019) A deep siamese-based plantar fasciitis classification method using shear wave elastography. IEEE Access 7:130999–131007
6. Gok G, Alp YK, Arikan O (2020) A new method for specific emitter identification with results on real radar measurements. IEEE Trans Inf Forensics Secur 15:3335–3346
7. Gong J, Xu X, Lei Y (2020) Unsupervised specific emitter identification method using radio-frequency fingerprint embedded InfoGAN. IEEE Trans Inf Forensics Secur 15:2898–2913
8. Goodfellow I, Bengio Y, Courville A (2016) Deep learning. MIT Press, USA
9. He B, Wang F (2020) Cooperative specific emitter identification via multiple distorted receivers. IEEE Trans Inf Forensics Secur 15:3791–3806
10. Hoad R, Carter NJ, Herke D, Watkins SP (2004) Trends in EM susceptibility of IT equipment. IEEE Trans Electromagn Compat 46(3):390–395
11. Hoad R, Lambourne A, Wraight A (2006) HPEM and HEMP susceptibility assessments of computer equipment. Proc Int Zurich Symp Electromagn Compat 168–171
12. Jin L, Liu G (2020) A method of radiation source identification based on DST-IFS. Proc IEEE Int Conf Inf Technol Big Data Artif Intell 438–442
13. Kingma D, Ba J (2014) Adam: a method for stochastic optimization. Proc Int Conf Learn Represent 156–160
14. Klambauer G, Unterthiner T, Mayr A (2017) Self normalizing neural networks. Adv Neural Inf Process Syst 30:972–981
15. Kreth A, Genender E, Doering O, Garbe H (2012) Identifying electromagnetic attacks against airports. Proc ESA Workshop Aerosp Electromagn Compat 1–5
16. Kulin M, Kazaz T, Moerman I, De Poorter E (2018) End-to-end learning from spectrum data: a deep learning approach for wireless signal identification in spectrum monitoring applications. IEEE Access 6:18484–18501
17. LeCun Y, Boser BE, Denker J, Henderson D, Jackel L (1990) Handwritten digit recognition with a back propagation network. Adv Neural Inf Process Syst 1990:396–404
18. Li D, Yang R, Li X, Zhu S (2020) Radar signal modulation recognition based on deep joint learning. IEEE Access 8:48515–48528
19. Liu S, Yan X, Li P, Hao X, Wang K (2018) Radar emitter recognition based on SIFT position and scale features. IEEE Trans Circuits Syst II Express Briefs 65(12):2062–2066
20. Liu Y, Xu H, Qi Z, Shi Y (2020) Specific emitter identification against unreliable features interference based on time-series classification network structure. IEEE Access 8:200194–200208
21. Maaten LV, Hinton GE (2008) Visualizing data using t-SNE. J Mach Learn Res 86:2579–2605
22. Paoletti U (2020) Broadband electromagnetic noise source identification using modulation frequency analysis. Proc Int Symp Electromagn Compat 1–5
23. Qian Y, Qi J, Kuai X, Han G, Sun H, Hong S (2021) Specific emitter identification based on multi-level sparse representation in automatic identification system. IEEE Trans Inf Forensics Secur 16:2872–2884
24. Rossi A, Hosseinzadeh M, Bianchini M, Scarselli F, Huisman H (2021) Multi-modal siamese network for diagnostically similar lesion retrieval in prostate MRI. IEEE Trans Med Imaging 40(3):986–995
25. Satija U, Trivedi N, Biswal G, Ramkumar B (2019) Specific emitter identification based on variational mode decomposition and spectral features in single hop and relaying scenarios. IEEE Trans Inf Forensics Secur 14(3):581–591
26. Standard: International Electrotechnical Commission (2006) CISPR 16–1–1: Specification for radio disturbance and immunity measuring apparatus and methods – Part 1–1: Radio disturbance and immunity measuring apparatus – Measuring apparatus. IEC Standard CISPR 16–1–1, 1-76.
27. Shi D, Gao Y (2013) A new method for identifying electromagnetic radiation sources using backpropagation neural network. IEEE Trans Electromagn Compat 55(5):842–848
28. Tan K, Yan W, Zhang L, Tang M, Zhang Y (2021) Specific emitter identification based on software-defined radio and decision fusion. IEEE Access 9:86217–86229
29. Wang B, Wang D (2019) Plant leaves classification: a few-shot learning method based on siamese network. IEEE Access 7:151754–151763
30. West NE, Shea TO (2017) Deep architectures for modulation recognition. Proc IEEE Int Symp Dyn Spectr Access Netw 1–6
31. Wong LJ, Headley WC, Michaels AJ (2019) Specific emitter identification using convolutional neural network-based IQ imbalance estimators. IEEE Access 7:33544–33555
32. Xiao Y, Zhu F, Zhuang S, Yang Y (2022) A New Neural Network Based on CNN for EMIS Identification. Journal of electronic testing-theory and application 38(1):77–89
33. Yang J, Zou H, Zhou Y, Xie L (2019) Learning gestures from WiFi: a siamese recurrent convolutional architecture. IEEE Internet Things J 6(6):10763–10772
34. You W, Zhang H, Zhao X (2021) A siamese CNN for image steganalysis. IEEE Trans Inf Forensics Secur 16:291–306
35. Zhang F, Hu C, Yin Q, Li W, Li H, Hong W (2017) Multi-aspect-aware bidirectional LSTM networks for synthetic aperture radar target recognition. IEEE Access 5:26880–26891
36. Zhang J, Wang F, Dobre OA, Zhong Z (2016) Specific emitter identification via Hilbert-Huang transform in single-hop and relaying scenarios. IEEE Trans Inf Forensics Secur 11(6):1192–1205
37. Zhang Q, Guo Y, Song Z (2021) Dynamic curve fitting and BP neural network with feature extraction for mobile specific emitter identification. IEEE Access 9:33897–33910
38. Zhao X, Wen Z, Pan X, Ye W, Bermak A (2019) Mixture gases classification based on multi-label one-dimensional deep convolutional neural network. IEEE Access 7:12630–12637

Ying-Chun Xiao received the B.S. degree in electronic information science and technology from Lanzhou University of Technology, Lanzhou, China, in 2012. She is currently a lecturer at Lanzhou City University. At the same time she is working toward the Ph.D. degree in electrical engineering at Southwest Jiaotong University, Chengdu, China. Her research interests include electromagnetic environment test and evaluation, electromagnetic compatibility analysis and design, and identification and location of electromagnetic interference sources.

Feng Zhu received the Ph.D. degree in railway traction electrification and automation from Southwest Jiaotong University, Sichuan, China, in 1997. He is currently a Full Professor in the School of Electrical Engineering, Southwest Jiaotong University. His current research interests include locomotive over-voltage and grounding technology, electromagnetic theory and numerical analysis of electromagnetic field, and electromagnetic compatibility analysis and design.

Shengxian Zhuang received his M.S. and Ph.D. degrees, respectively, at Southwest Jiaotong University and the University of Electronic Science and Technology of China in 1991 and 1999. From 1999 to 2003, he did postdoctoral research at Zhejiang University and Linkoing University of Sweden. He was a visiting professor at Paderborn University in Germany in 2005 and at the University of Leeds, UK in 2017. He is currently working with the School of Electrical Engineering at Southwest Jiaotong University as a professor. His research interests include power conversion for sustainable energies, motor control and drive systems, power electronics and systems integration, modeling, diagnosis, and suppression of electromagnetic interference of power electronic converters.

Yang Yang received her bachelor's degree in measurement and control technology and instrumentation from Shaanxi University of Science and Technology in 2011 and her master's degree in control theory and control engineering from Northwestern Polytechnical University in 2014. She is currently working toward a Ph.D. degree in electrical engineering at Southwest Jiaotong University, Chengdu, China. Her research interests include electromagnetic environment testing and evaluation, electromagnetic compatibility analysis and design, and electromagnetic compatibility problems in the field of railway power supply and rail transit.